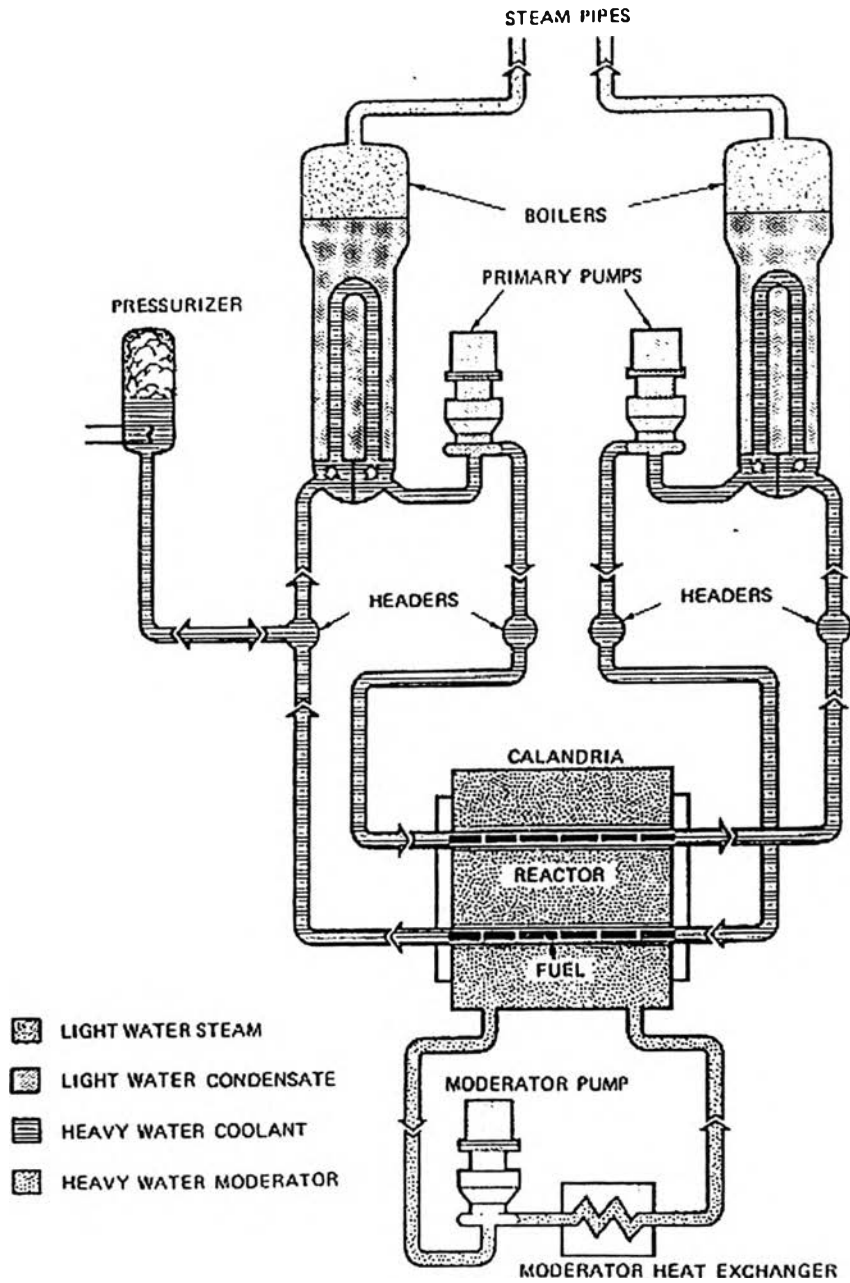


CHAPTER II

LITERATURE REVIEW

2.1 CANDU Primary Coolant Loop

In the core of the CANDU reactor, there is a fission controlled reaction like any other nuclear reactor. However CANDU reactor is fuelled with natural uranium in the form of uranium oxide (UO_2) clad in Zircaloy. The fuel is contained in 380 Zr 2.5%Nb pressure tubes. Heat from the nuclear reaction is removed by heavy water (D_2O) which is the primary coolant. The heat is carried by the reactor coolant through carbon steel pipes into headers which are also carbon steel to the steam generator. Within the steam generator which contains nickel alloy tubes, the secondary side light water is changed into saturated steam by heat from the coolant. The coolant is returned through the feeder inlet pipes to the reactor core. The pressure tubes in the reactor core are connected to feeders via end fittings which are designed for convenient re-fuelling. A Grayloc connector is used to attach each feeder to its fuel channel end fitting. The reactor coolant circulation is called the primary coolant loop as shown in Figure 2.1. The CANDU primary coolant loop consists of three main components: the reactor core, the steam generators and the piping system.



CANDU REACTOR SIMPLIFIED FLOW DIAGRAM

Figure 2.1 Primary coolant loop (Atomic Energy of Canada Limited, 1973).

The summary of material construction of each component is shown in Table 2.1

Table 2.1 Material construction summary.

Reactor core	Zirconium alloy
Steam generator *	Nickel alloy - Monel 400 - Inconel 600 - Incoloy 800
Piping	SA-106 Grade B Carbon Steel

*depends upon CANDU model.

The primary coolant enters the reactor core at 265°C and removes heat from the nuclear reaction. It leaves the core at 310°C with average steam quality 2% (Lister *et al.*, 1998). Chemicals are added to the coolant for two major requirements : 1.) to minimize dissolved oxygen by adding dissolved hydrogen (D₂) 3-10 cm³/kg at STP and 2.) to maintain alkalinity by adding lithium hydroxide (lithia) (Barber and Lister, 1982 and Lister *et al.*, 1998,). From the single-phase study of Lister, Arbeau and Johari, it is suggested that the pH be controlled between 10.4-10.6 measured at room temperature. Moreover, they suggested a conductivity range of 2.2-3.5 mS/m, chlorine ion concentration of less than 300 µg/kg and dissolved O₂ of less than 4 µg/kg (Lister *et al.*, 1994).

2.2 Material Composition

Carbon steel was selected as a construction material for feeders and headers based on work of Videm and Aas (Videm and Aas, 1963). They stated that the corrosion rate decreased with time up to 4000 hours at about 4.64-6.24 µm/yr (30-40 µg/dm³-month). After 4000 exposure hours, the rate was about 0.16 µm/yr (1mg/dm³-month) for a high pH system. From Figure 2.2, it is

indicated that the corrosion rate is $7.74 \mu\text{m}/\text{yr}$ ($50 \text{ mg}/\text{cm}^2\text{-month}$) at exposure hour of 1000 at high pH. It was concluded that carbon steel can be used as the construction material of CANDU feeder pipes for long term operation. This selection reduced the capital investment for a plant significantly.

Videm and Aas found that most corrosion products at high pH were particles which can be filtered off, but cannot be removed by filters or ion exchangers in a neutral system because of corrosion products as ions and colloids.

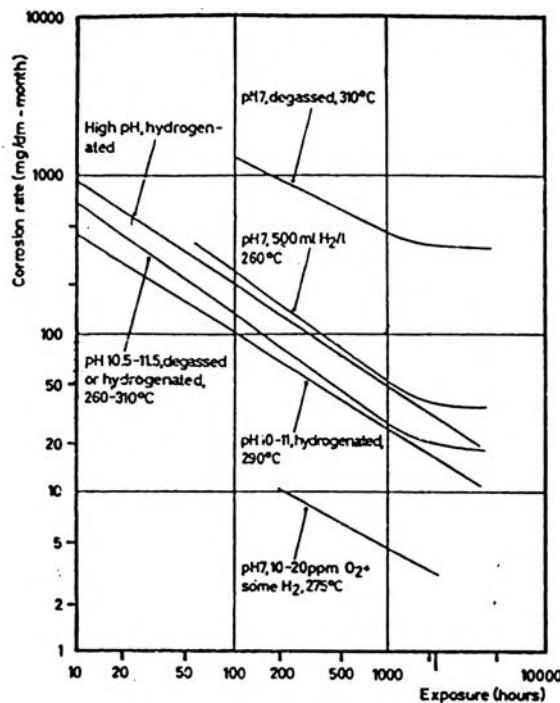
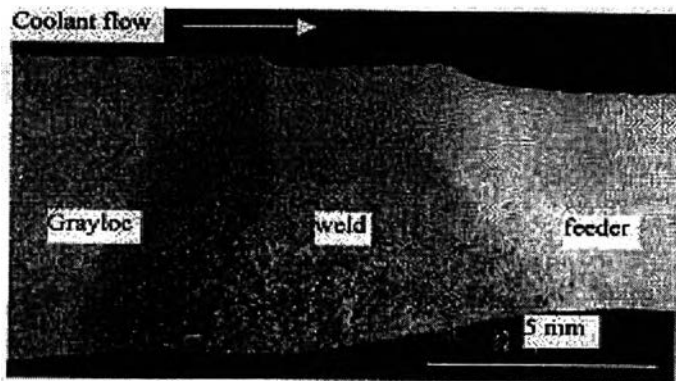


Figure 2.2 Corrosion rate of mild steel versus exposure (Videm and Aas, 1963).

Carbon steel A 106-B contains iron as the main component with small amounts of carbon, chromium, cobalt, manganese, nickel, copper and other elements' traces (ASTM A-106). The amount of chromium in steel is an important factor in the thinning phenomenon because chromium can form an oxide that protects the surface (Robertson and Forrest, 1991).

ASTM A 106 limits the chromium content in carbon steel A 106 grade B to not more than 0.40%. For CANDU reactors, the chromium content was reduced to a low level to achieve low cobalt content. To minimize activity transport in the primary system, it is necessary to have low cobalt in the system. This leads to Cr concentrations of 0.02-0.03% for feeders (Lister *et al.*, 1998). Their work also indicated that there was minor thinning for the Grayloc hub which contained 0.13%Cr and 0.07%Cr for weld joining. From Figure 2.3, it is shown that the thinning increases stepwise to the pipe. This indicates that when chromium content decreases, the thinning increases.

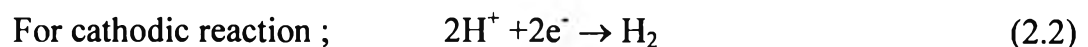
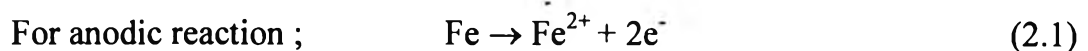
Figure 2.3 Section through piping and Grayloc hub : outlet feeder S08



removed from Point Lepreau (Lister *et al.*, 1998).

2.3 Corrosion Mechanism and Species in the System

The corrosion of metals in an aqueous system involves two or more electrochemical reactions. Lang (2000) gave a detailed description of the mechanisms. The carbon steel piping corrosion can be represented by two simple reactions :



Iron metal corrodes and converts into the iron ion ferrous (Fe^{2+}) form. About 50% of dissolved iron is converted into oxide of iron as magnetite (Fe_3O_4) at the metal/oxide interface (Potter and Mann, 1962; and Tomlinson, 1981). The layer of this oxide is called the inner oxide layer. The remainder of the dissolved iron diffuses outward through the oxide layer and form oxide as outer oxide layer. This double layer is called duplex of magnetite or Potter-Mann layer (Potter and Mann, 1962) as shown in Figure 2.4. The oxides in the inner layer are fine crystal overlaid with coarse octahedral crystals in the outer oxide layer (Robertson and Forrest, 1991).

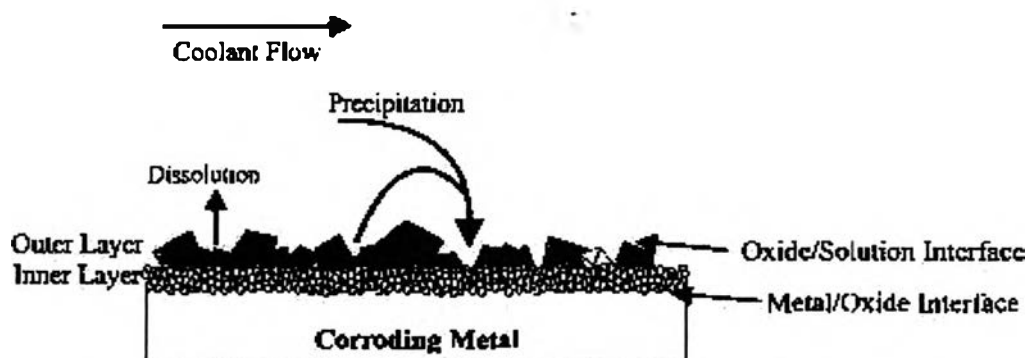


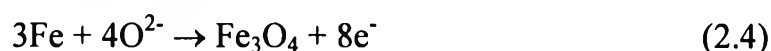
Figure 2.4 Duplex of magnetite, Potter-Mann layer (Lang, 2000).

Tomlinson proposed two possibilities to form the inner oxide layer depending on the species being transferred to the oxygen source for the reaction.

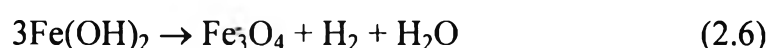
If water molecules are the diffusing species ;



If O^{2-} and H^+ are the diffusing species ;

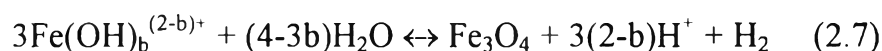


Sanchez-Caldera *et al.* (1988) stated that hydroxide produced in the first step of iron oxidation can form magnetite according to Eq. 2.6.



Additionally, the ferrous hydroxide can transform into magnetite through the Schikorr reaction at high temperatures, above 100°C, and the rate of formation will be faster at higher temperatures (Berge *et al.*, 1976).

Schikorr reaction ;



If the system is unsaturated, magnetite can dissolve through the reverse of the Schikorr reaction (Berge *et al.*, 1976). This leads to the following species: Fe^{2+} , $\text{Fe}(\text{OH})^+$, $\text{Fe}(\text{OH})_2$, $\text{Fe}(\text{OH})_3^-$ (Sanchez-Caldera *et al.*, 1988; and Robertson and Forrest, 1991) depending on the pH of system (Lang, 2000).

The corroded iron species forms an inner oxide layer immediately at the metal/oxide interface. The rest of the dissolved iron diffuses from the metal/oxide interface to the oxide/solution interface. Meanwhile, H_2O and O^{2-} or H_2 are transported from the oxide/solution interface to metal/oxide interface. At the oxide/solution interface, the iron ions go into the solution until the solution is saturation. Thereafter, these iron ions will form an outer oxide layer by precipitating as Eq. 2.7.

The important reactions and species transported are identified in Figure 2.5. At point 1, the iron metal corrodes and converts into iron ions at the anodic surface. H_2 evolution at point 3 (cathodic surface) is the result of metal corroding. Some of the iron (1-f) precipitate at point 2. The remainders (f) diffuse to the bulk solution and form the outer oxide through the Schikorr reaction when the bulk solution is saturated with iron ions. Hydrogen ions are formed from the Schikorr reaction caused by the outer oxide layer formation and diffuse from the oxide/solution interface to form H_2 at point 4.

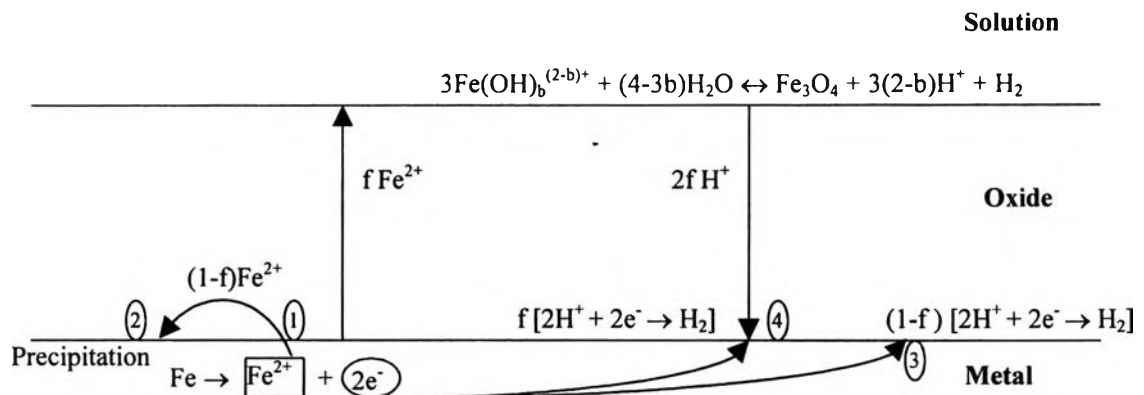


Figure 2.5 Diagram of species transportation and corrosion mechanism.

From Figure 2.5, there are many species involved in thinning phenomenon that will be mentioned subsequently.

2.3.1 Magnetite

Magnetite is an oxide of iron and is observed on metal such as carbon steel in CANDU (Lister *et al.*, 1994). This magnetite (Fe_3O_4) on carbon steel is an inverse spinel (Wells, 1975). It is the most common oxide form on stainless steel in high pressure and high temperature system (Basque, 1997). The unit cell of the spinel consists of 32 oxygen ions, 8 divalent cations and 16 trivalent cations. Thus, there are 32 O^{2-} , 8 Fe^{2+} and 16 Fe^{3+} in a unit cell for magnetite spinel.

There are two types of spinel depending upon the distribution of cations in a spinel:

1) normal spinel : divalent cations occupy only tetrahedral sites, meanwhile, trivalent cations occupy octahedral.

2) inverse spinel : one-half of trivalent cations (8 ions) occupied tetrahedral sites and the rest are arranged with divalent ions at random in the 16 octahedral positions (Wells, 1975).

There are two layers of magnetite: inner layer and outer layer. In the inner layer, magnetite is fine because it grows in a confined space. The magnetite is coarse in the outer layer because it grows without volume constraint. Magnetite layer can protect the surface from thinning, especially the inner oxide layer which is coherent.

2.3.2 Dissolved Iron

Most of the product of magnetite dissolution and metal corrosion is in the form of ferrous and goes into the solution as positive charges as Fe^{2+} or FeOH^+ . Tomlinson (1981) stated that corrosion was controlled by diffusion of O^{2-} and Fe^{2+} . The same idea as Robertson (1989) and Effertz (1972) is that diffusion of dissolved iron is the rate limiting step. There are two major ways for diffusion through oxide layers : 1) by the solution state through pores and 2) by solid state diffusion such as through lattice or along grain boundaries. Johari proposed 2 possible models for dissolved iron transportation: 1) pore solution and 2) grain boundaries.

2.3.2.1 *Pore Solution Model*

Many authors indicated that dissolved metal diffuses outward through porous oxide to the solution (Tomlinson, 1981; Berge *et al.*, 1976; Castle and Mann, 1966; and Robertson, 1989). Castle and Mann (1966) stated that pores were formed by loss of iron to the environment. Because of the porous oxide, the pores provide the oxidant and water ingress as well as iron ions egress to the solution. The concentration gradient of dissolved iron across the oxide layer is the driving force for diffusion.

Robertson (1989) mentioned three deficiencies of this model.

1) The problem was about size of pores. He found that the pores did not all extend across the oxide. Furthermore, Tomlinson

(1981) found there was an absence of open pores more than 10\AA . Therefore, the pore size was too small to allow the iron to diffuse through these pores.

2) The problem concerned the similarity of corrosion rates of pure water and steam. It was found by several authors that the curve of corrosion rate constant in water and steam were the same as shown in Figure 2.6. This implied that aqueous corrosion in neutral water did not involve solution transport and was therefore the same as in steam oxidation. The diffusion mechanism in aqueous solution and in steam should thus be the same. Thus, iron ions should diffuse along grain boundaries to the solution.

3) The problem concerned the temperature dependence of the corrosion rate. It seemed that the order of magnitude of the temperature effect on the rate of oxide growth constant was too low because the activation energy for this in an aqueous solution was low. This problem was found in previous work (Castle and Masterson, 1966).

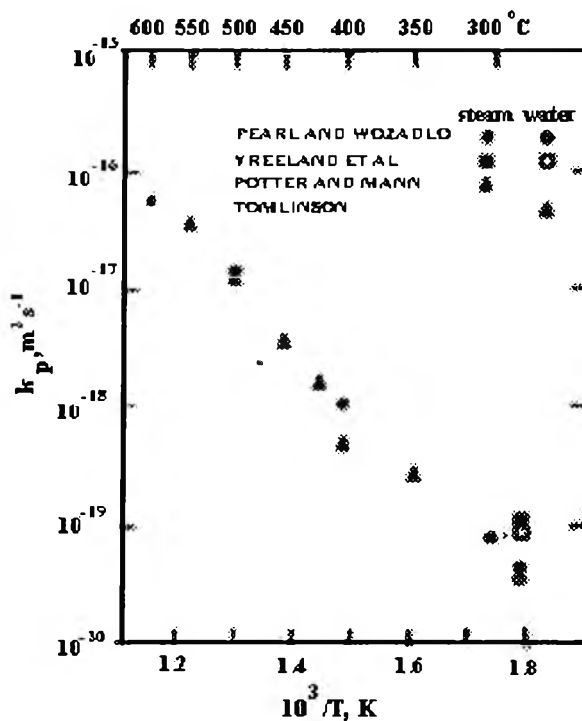


Figure 2.6 Corrosion rate constant for mild steel in pure water and steam (Robertson, 1989).

2.3.2.2 Grain Boundaries Model

The iron ions diffuse outward to the oxide/solution interface along grain boundaries in the oxide because of the gradient of iron ions. This occurs under conditions of local equilibrium and charge neutrality and is known as the Wagner theory (Robertson, 1989). Tomlinson (1981) proposed that the iron ions movement along grain boundaries might be explained by vacancy diffusion.

There are two defects that may occur in magnetite crystals: cation vacancies and cation interstitials. Fe^{2+} ion adding within a vacant octahedral interstice causes cation interstitial while the missing Fe^{2+} ion in an octahedral site causes cation vacancy. Both defects require charge neutrality. 2Fe^{3+} ions are converted to Fe^{2+} for interstitials and 2Fe^{2+} ions are converted to Fe^{3+} for vacancies. These changes cause intermediate species such as $\gamma\text{-Fe}_2\text{O}_3$ lattice or FeO lattice (Robertson, 1989). This charge neutrality involves the current connected with the flux of Fe^{2+} ions through the oxide film to be matched by a compensating electric current. Meanwhile, the pore solution model is considered without the effect of electrochemistry (Robertson, 1989).

The species transportation including dissolved iron transportation inside the oxide layer is illustrated in Figure 2.7.

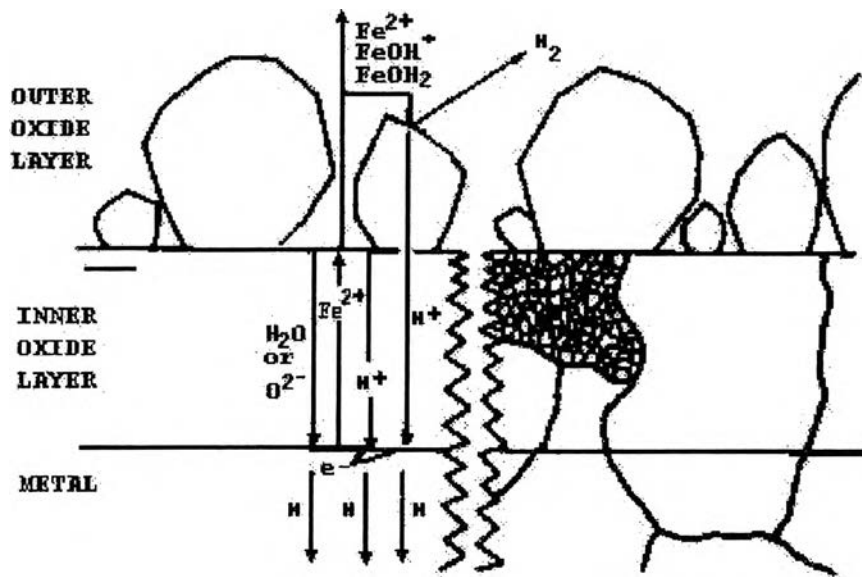


Figure 2.7 Transportation in oxide (Tomlinson, 1981).

2.3.3 Hydrogen

Hydrogen diffuses through the oxide layer as a hydrogen molecule, or as a hydrogen ion (H^+). Hydrogen ion diffuses inwards to the metal/oxide interface to neutralize the charge in oxide layer. H^+ is reduced at the metal/oxide interface by the cathodic reaction. Tomlinson (1981) observed that up to 90% of the hydrogen is generated at the metal/oxide interface. In contrast, Robertson stated that about half of the hydrogen evolution would occur at the metal/oxide interface, and the other half would occur at the oxide/solution interface (1989).

2.3.4 Oxygen

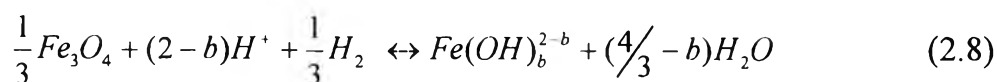
The magnetite protective film forms at the metal/oxide interface by a combination of oxygen and iron metal according to Eq. 2.4. Oxygen has to be transported from the oxide/solution layer to metal/oxide layer. There are many ideas concerning the forms of transported oxygen. Effertz (1972) proposed that oxygen moved inwards to metal/oxide interface as oxygen ions

(O^{2-}) along grain boundaries. Tomlinson (1981) supported Effertz's opinion, in addition, he thought that H_2O could diffuse inwards as an oxygen source. His thought was supported by Abdulsalam and Stanley (1992). Tomlinson stated the possibility that the mechanism depended on the detailed microstructure of the oxide layer. If the pores size is greater than 1 nm in diameter, the molecule of water can diffuse through the oxide layer. Additionally, Robertson observed that the oxygen atom diffused through the oxide layer instead of oxygen ions since lattice diffusion of O^{2-} ions is much too slow to account for the inner layer growth rate (1989).

2.4 Oxide Solubility

Oxide solubility is one of major effects on corrosion. When solubility is low, the solution achieves saturation easily. If solubility is high, a large amount of oxide can dissolved into the solution. It is believed that magnetite solubility depends on temperature and pH as well as solution composition. Many authors confirmed this (Sweeton and Baes, 1970; Balakrishnan, 1977; and Tremaine and Leblanc, 1980). Moreover, solubility is affected by the electrochemical potential. This will be discussed later in more detail.

Sweeton and Baes (1970) considered only ferrous species (Fe^{2+} , $FeOH^+$, $Fe(OH)_2$, and $Fe(OH)_3^-$) from Fe_3O_4 according to Eq. 2.8.



The effect of these species is indicated in Figure 2.8.

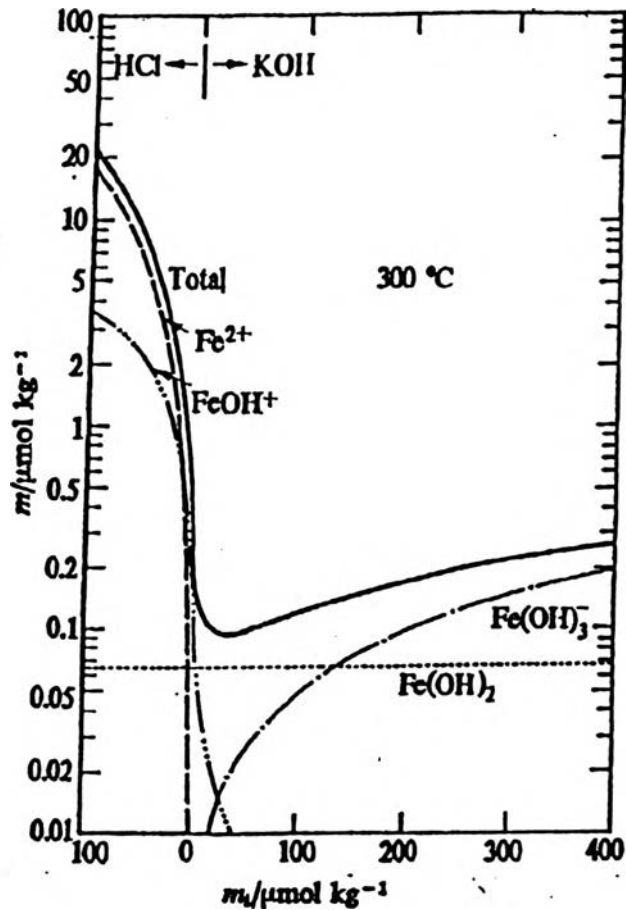
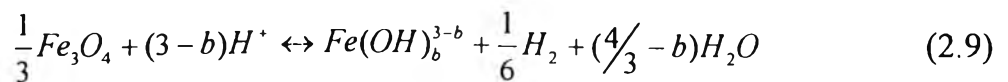


Figure 2.8 Distribution of species after equilibrating Fe_3O_4 at 300°C (Sweeton and Baes).

In addition, Tremaine and Leblanc (1980) proposed not only soluble ferrous species but also ferric species to determine magnetite solubility. Thus, there are six species in the solution: Fe^{2+} , $\text{Fe}(\text{OH})^+$, $\text{Fe}(\text{OH})_2$, $\text{Fe}(\text{OH})_3^-$, and $\text{Fe}(\text{OH})_4^-$ corresponding to the reaction 2.8 and 2.9.



From Figure 2.9, at 300°C and $\text{pH}_{25^\circ\text{C}}$ of 10 which is close to the primary coolant loop system conditions, $\text{Fe}(\text{OH})_2$ is a predominant species.

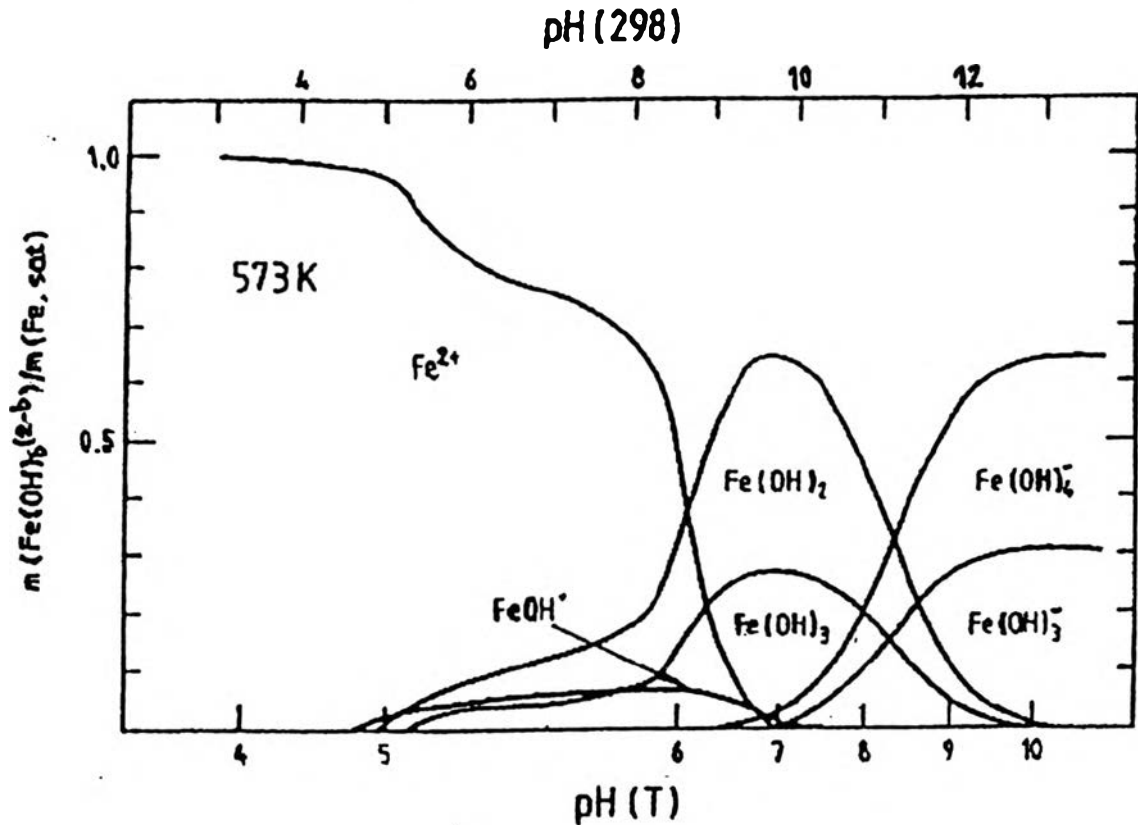


Figure 2.9 Predominant species diagram at 300°C (Tremaine and Leblanc, 1980).

2.4.1 Temperature Effect

Magnetite solubility strongly depends on temperature and the pH of the system. The primary coolant loop of the CANDU, system is operated at a pH of approximately 10 where the solubility increases with temperature as illustrated in Figure 2.10. Therefore, the coolant becomes unsaturated after flowing through the reactor core and having the temperature elevated from 265°C to 310°C. The increase of magnetite solubility will cause outer oxide dissolution, so the outlet feeder pipes are much more susceptible to thinning than the inlet feeder pipes.

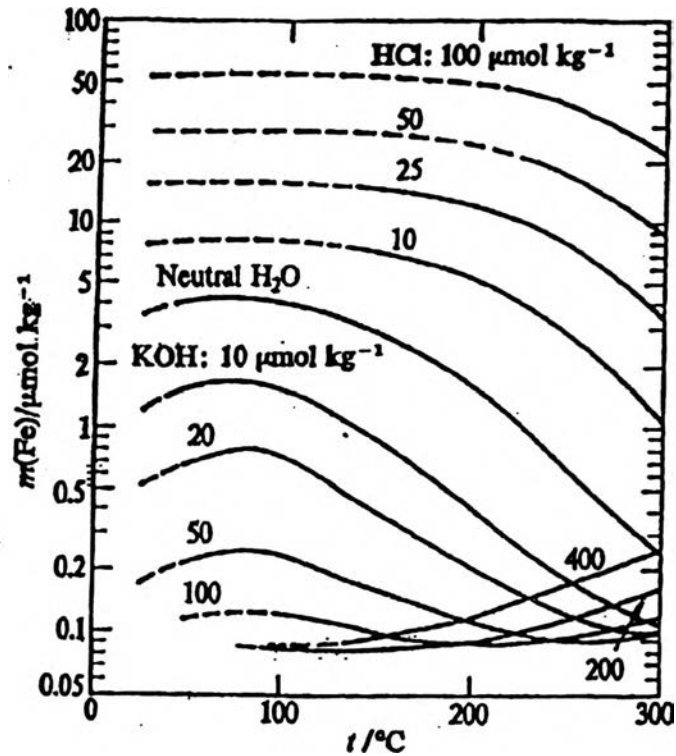


Figure 2.10 Solubility of Fe_3O_4 in aqueous solutions saturated with H_2 at 1 atm and 25°C (Sweeton and Baes, 1970).

2.4.2 H_2 Effect

According to Eq. 2.7, it is found that the hydrogen concentration affects the amount of $\text{Fe}(\text{OH})_b^{(2-b)+}$ in the system. According to the Schikorr reaction, the equilibrium constant can be calculated from Eq. 2.10.

$$K = \frac{[\text{Fe}(\text{OH})_b^{(2-b)+}]}{[\text{H}^+]^{2-b} [\text{H}_2]^{1/3}} \quad (2.10)$$

If the pH is constant, Eq. 2.10 can be rewritten as Eq. 2.11;

$$K' = \frac{[\text{Fe}(\text{OH})_b^{(2-b)+}]}{[\text{H}_2]^{1/3}} \quad (2.11)$$

From Eq. 2.11, it is indicated that the concentration of ferrous species increases with increasing hydrogen species. This means that local solubility of magnetite increases with the power 1/3 of H₂ concentration. This statement was confirmed by Berge *et al.*(1976) and Tomlinson (1981).

In the inner oxide, hydrogen is generated from corroding metal and the precipitation of dissolved iron to be magnetite. In contrast, hydrogen is formed only by precipitation in the outer oxide layer. This is the reason for the higher hydrogen concentration at the metal/oxide interface than at the oxide/solution interface. Consequently, the driving force for mass transfer of iron ions is greater.

2.5 Erosion-FAC

The combination of flow action and corrosion results in flow-assisted corrosion (FAC). FAC is the acceleration or increase in rate of the deterioration metal surface (Fontana, 1986). Thus, the velocity of the fluid plays an important role in erosion corrosion. The concept of flow effects on corrosion was introduced in the 1950's.

The flow-assisted corrosion causes an increase in corrosion rate at a high velocity by mass transfer and phase transport. Moreover, fluid flow can cause erosion corrosion and cavitation. Heitz (1991) divided the flow-assisted corrosion into four types as illustrated in Figure 2.11: mass transport-controlled corrosion, phase transport-controlled corrosion, cavitation corrosion and erosion corrosion.

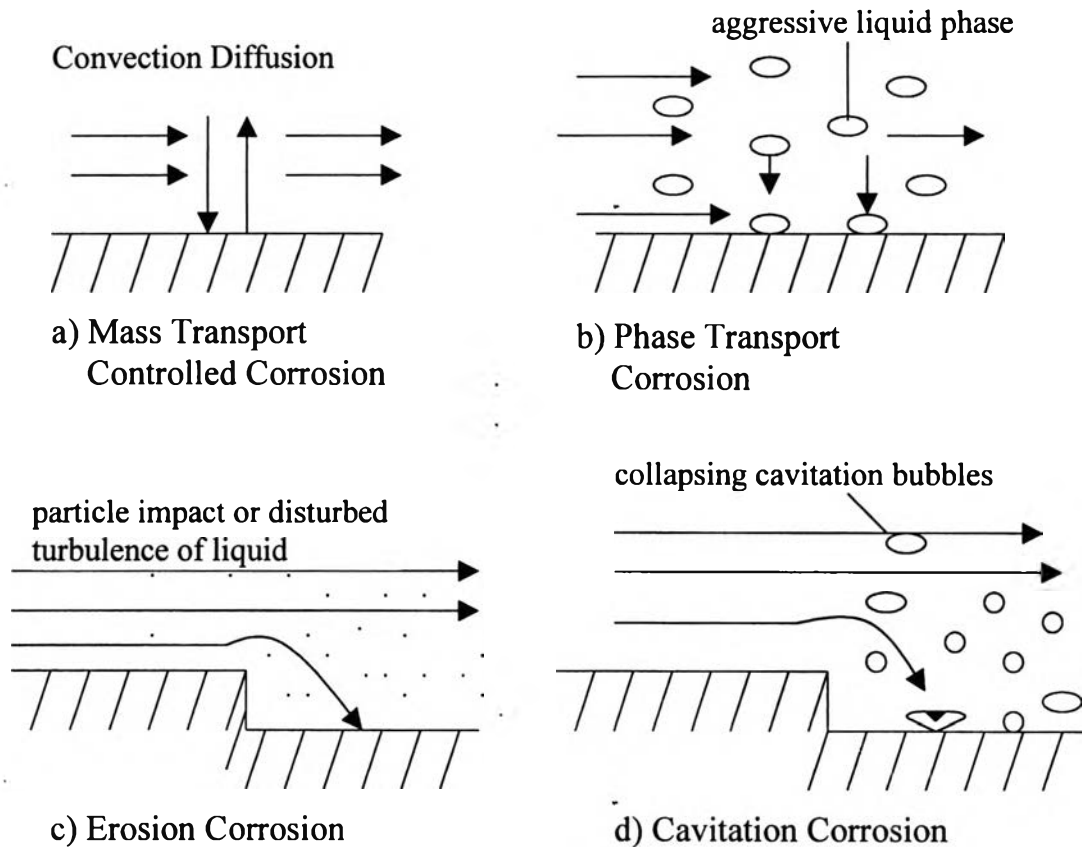


Figure 2.11 Four main mechanisms of flow-assisted corrosion (Heitz, 1991).

In a practical way, it is always a mixed control of mass transfer and reaction at surface.

Mass transfer and the kinetics of oxide dissolution are the important mechanisms affecting FAC. Bignold *et al.* (1983) and Abdulsalam *et al.* (1992) proposed the overall rate for erosion-corrosion.

overall resistance = mass transfer resistance + kinetics resistance

$$\frac{1}{R_T} = \frac{1}{R_{MT}} + \frac{1}{R_K} \quad (2.12)$$

where R_T = overall rate

- R_{MT} = mass transfer limited rate
 R_K = kinetics rate of oxide dissolution.

Assuming that the kinetics of oxide dissolution vary with temperature according to an Arrhenius expression.

$$R_K = R_o \exp(-E_K / RT) \quad (2.13)$$

- where R_o = R_K at $T=\infty$
 E_K = the activation energy .
 R = gas constant (8.314 J/mol K)
 T = temperature.

If mass transfer is as controlling mechanism,

$$R' = R_{MT} = m_c(C_s - C_b) \quad (2.14)$$

- Where m_c = mass transfer coefficient
 C_s = concentration at oxide solution interface
 C_b = concentration in bulk solution.

Figure 2.12 indicates the regimes that depend upon velocity. If mass transfer is controlling the corrosion rate increases with velocity ($m_c < k_c$, the potential-dependent rate constant for the electron transfer). This is the low velocity region. If the velocity is high, the corrosion rate is essentially independent of velocity. In this region kinetics control the corrosion rate.

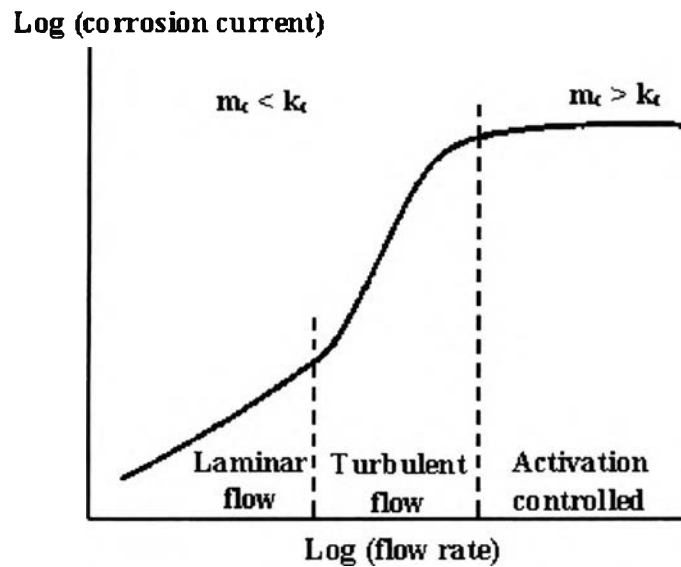


Figure 2.12 The relation between corrosion current and flow rate in different in controlled step regions.

The mass transfer coefficient varies with hydrodynamic conditions such as flow velocity according to the following.

$$Sh = a Re^b Sc^c \quad (2.15)$$

- where
- Sh = Sherwood number = hd/D
 - Re = Reynolds number = $d\rho u/\mu$
 - Sc = Schmidt number = $\mu/\rho D$
 - h = mass transfer coefficient
 - d = diameter
 - D = diffusion coefficient
 - ρ = fluid density
 - u = fluid velocity
 - μ = fluid viscosity

b = constant

c = constant.

From Eq. 2.15, it is concluded that the mass transfer coefficient increases with velocity. Thus, when the flow velocity is low, the system is dominated by a mass transfer-controlled mechanism. On the other hand, high velocities cause high mass transfer, consequently, high corrosion rate occurs as shown in Figure 2.12.

Erosion corrosion is a combination of flow-assisted mechanical forces and chemical processes. This implies that erosion corrosion is a chemo-mechanical process. The mechanical action is composed of: shear stresses and pressure variations by the high velocity fluid, and particle impact in multiphase flows.

Cavitation is a mechanical effect which occurs in the system with high velocity fluid undergoing rapid pressure changes. This effect destroys the protective film.

Heitz (1991, 1996) proposed the simple expression to indicate the correlation between corrosion rate and velocity.

$$w = \text{const} \times u^a \quad (2.16)$$

where w = corrosion rate

u = flow velocity

a = exponent constant which depends on mechanisms of the system.

Additionally, Stack *et al.*(1995) proposed a similar expression to that proposed by Heitz.

$$E = Kv^n f(\theta) \quad (2.17)$$

where E = erosion rate
 K = constant
 v = flow velocity
 n = exponent
 θ = impact angle.

Figure 2.13 is similar to Figure 2.12, however it illustrates the relationship between erosion corrosion and velocity. It is indicated that erosion corrosion rate increases with fluid velocity and increases more rapidly at higher velocities. The velocity at which erosion-corrosion starts to increase rapidly is called critical flow velocity (V_c). Thus, the critical flow velocity is the highest permissible flow velocity within the safe region. This safe region comprises both the laminar flow regime and part of the turbulent flow regime.

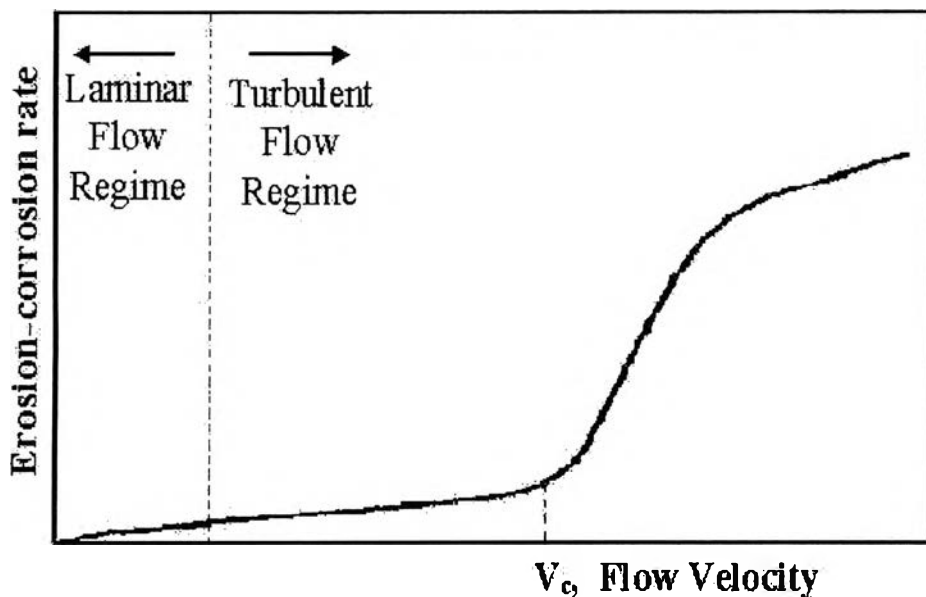


Figure 2.13 Flow velocity effect on erosion-corrosion rate (Stack *et al.*, 1995).

From Figure 2.13, the velocity dependence can be divided into various regimes. Stack *et al.* (1995) determined the exponent of Eq. 2.17 of low alloy steel in aqueous systems. At low velocity region (0-25 m/s), exponent(n) is

0.78. The exponent is 3.3 for an intermediate velocities (25-35 m/s), and the exponent decreases at the velocities above 35 m/s.

Shear stress has a significant effect on erosion corrosion, especially, wall shear stress. Higher wall shear stress creates a higher mass transfer rate and thus a higher corrosion. The high wall shear stress causes the oxide layer to shear off and spall out from the surface. Wall shear stress is a function of velocity. It increases with velocity according to the Eq. 2.18.

$$\tau_w \propto U^a \quad (2.18)$$

where τ_w = wall shear stress
 U = mean velocity of fluid
 a = constant exponent factor.

For cylindrical pipe,

$$\tau_w = \frac{1}{2} f \rho U^2 \quad (2.19)$$

where ρ = fluid density
 f = friction factor.

The friction factor is a function of Reynolds number and its value can be determined from Moody Diagram.

$$f = f(\text{Re}) \quad (2.20)$$

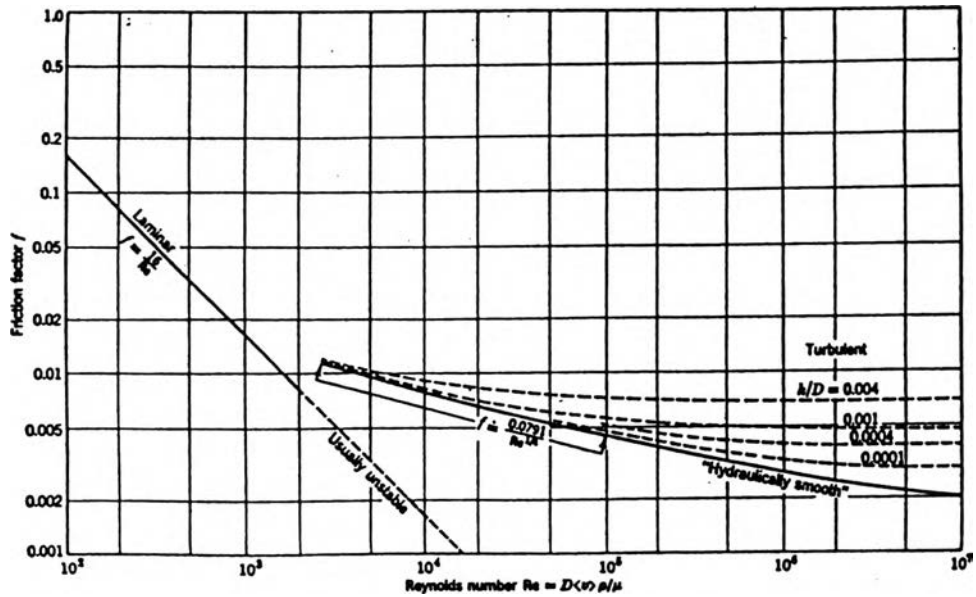


Figure 2.14 Moody Diagram.

By approximation for turbulent flow

$$f = 0.0791/Re^{1/4} \quad (2.21)$$

The intensity of turbulence is a measure of the turbulent disturbance. The intensive turbulence near the wall can affect corrosion by disturbing the mass transfer and by breaking up the protective oxide layer (Nešić and Postlethwaite, 1991). The main source of turbulence is the shear stress at the wall. Thus, the intensity of turbulence has a similar effect as wall shear stress on erosion-corrosion.

2.6 Surface Roughness and Geometry

Surface roughness and geometry can influence the mass transfer coefficient which is one of the important parameters controlling erosion-

corrosion. When metal is roughened, there is an increase in the mass transfer coefficient, consequently, an increase in mass loss.

The mass transfer coefficient can be determined by the equation (Eq. 2.15). Postlethwaite and Lotz (1988) presented the correlation for a smooth surface as

$$Sh = 0.0089 Re^{0.89} Sc^{0.33} \quad (2.22)$$

Furthermore, for the effect of the surface roughness, they established the correlation of mass transfer coefficient for both the smooth and rough surfaces. The ratio of the rough to smooth surface mass transfer coefficients, k_r/k_s , is a function of the Schmidt number.

$$k_r/k_s = 1.82 Sc^{0.1} (e^+)^{-0.17} \quad (2.23)$$

where e^+ = dimensionless roughness height.

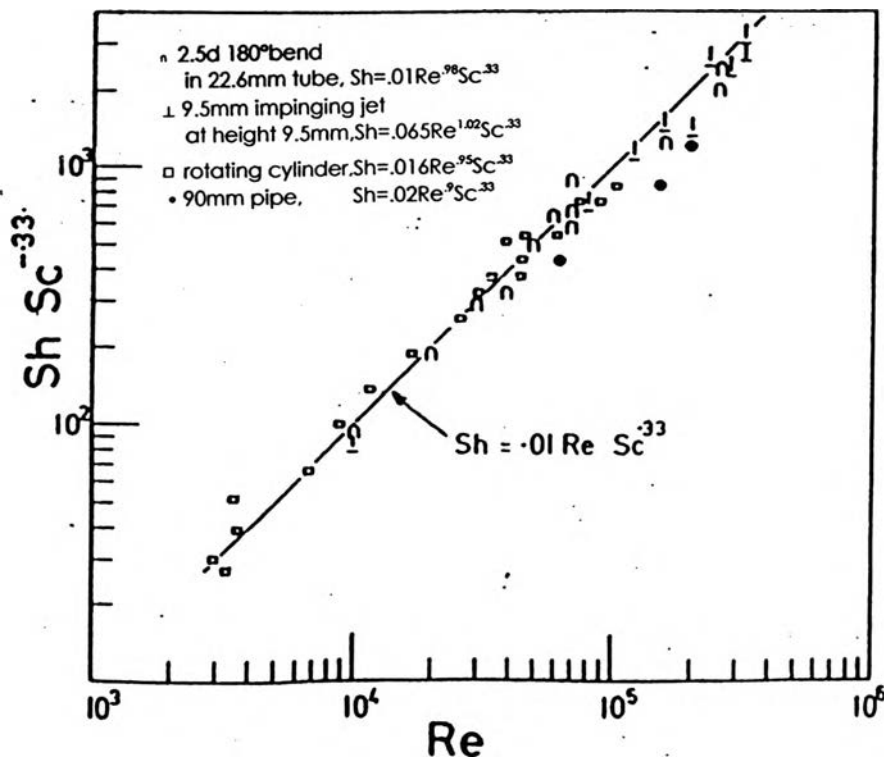


Figure 2.15 Mass transfer from rough surfaces (Poulson, 1990).

Poulson (1990) concluded that mass transfer from a rough surface is linearly related to the Reynolds number as illustrated in Figure 2.15.

Surface roughness also affects the friction factor that influences the shear stress as described in section 2.6. If the circular tubes are rough, high pressure drops are required in the turbulent region as shown in Figure 2.15.

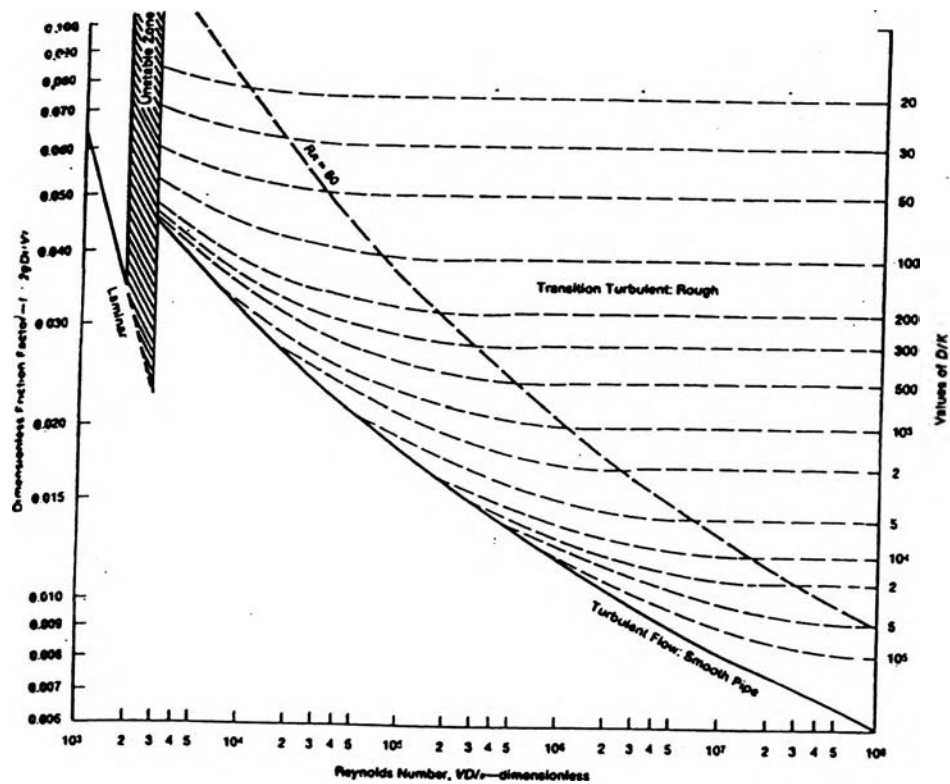


Figure 2.16 Roughness effect for circular tube (Lamont, 1981).

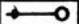



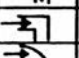

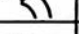

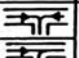
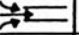
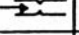




FLOW PATTERN		REFERENCE VELOCITY	R_c
PRIMARY FLOW STAGNATION POINTS	 AT PIPES	VELOCITY OF INITIAL FLOW (UPSTREAM OF STAGNATION OBSTACLE)	1
	 AT BLADES		1
	 AT PLATES		1
	 IN PIPE JUNCTIONS		1
	 IN PIPE JUNCTIONS		0.8
SECONDARY FLOW STAGNATION POINTS	 R/D = 0.5	FLOW VELOCITY	0.7
	 R/D = 1.5		0.4
	 R/D = 2.5		0.3
	 BEHIND PIPE JOINTS		0.2
STAGNATION POINTS DUE TO VORTEX FORMATION	 BEHIND SHARP EDGED ADMISSION PIPES	FLOW VELOCITY	0.2
	 AT AND BEHIND BARRIERS		0.2
NO STAGNATION POINTS	 IN STRAIGHT PIPES	FLOW VELOCITY	0.04
	 IN UNLIGHT HORIZONTAL TURBINE JOINTS	VELOCITY CALCULATED FROM PRESSURE DROP	0.08
COMPLICATED FLOW THROUGH TURBINE PART	 IN TURBINE GLAND SEAL	VELOCITY CALCULATED FROM PRESSURE DROP	0.08
	 AT AND ABOVE TURBINE BLADES AND AT DRAINAGE COLLECTING RINGS	AVERAGE CIRCUMFERENTIAL BLADE VELOCITY	0.3

Figure 2.17 Geometry factors (Henzel *et al.*, 1988).

The friction factor (f) is a function of the Reynolds number as well as the ratio of k to D in turbulent regress. This ratio (k/D) is known as of relative roughness. The friction factor increases with the k/D ratio, relative roughness, at the same flow rate. From Figure 2.16, the solid curve for a smooth pipe (hydraulically smooth) or for k value of zero.

The influence of geometry on material loss was mentioned by Henzel *et al.* (1988). They expressed geometry factors to describe this effect. These geometry factors are based on hydrodynamic conditions as shown in Figure 2.17 and the effect of geometry on thinning is illustrated in Figure 2.18.

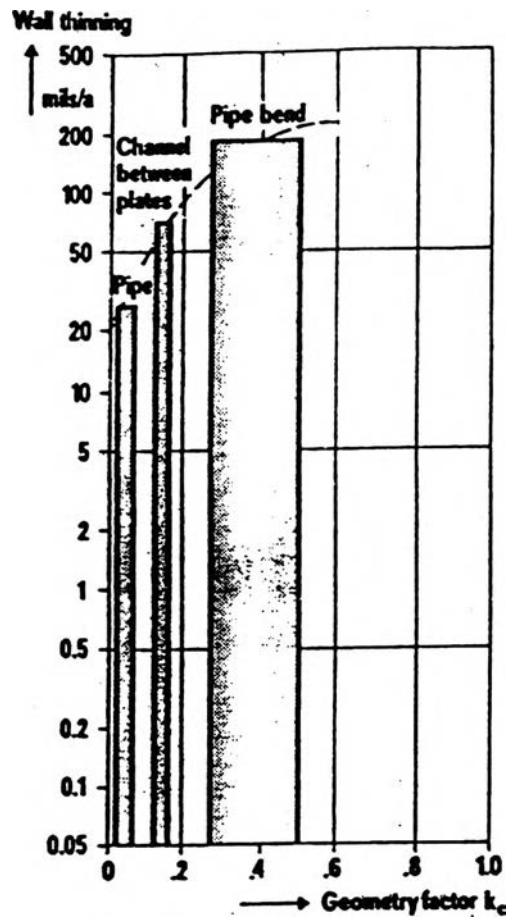


Figure 2.18 Geometry effect on wall thinning (Henzel *et al.* 1988).

The difference in geometries gives different mass transfer coefficients. This idea was confirmed by many works. For example, Poulson and Robinson (1988) studied the local mass transfer coefficient of 180° bends and gave the definition of the enhancement factor term as Eq. 2.24.

$$\text{enhancement factor} = \frac{\text{corrosion rate at bend}}{\text{corrosion rate of straight tube}} \quad (2.24)$$

It is found that the initial or smooth enhancement is less than 1.8 at Reynolds numbers up to 3×10^5 . The final or rough value (roughened bend) is a function of Reynolds number.

$$\text{rough enhancement factor} = 0.71 \text{Re}^{0.12} \quad (2.25)$$

2.7 Entrance Effect

The primary coolant flows from reactor core into the outlet feeder pipes. It leaves the end-fitting annulus and enters a grayloc hub as shown in Figure 2.19. The disturbed flow occurs in the entrance region of the outlet feeder pipes where the bend involved is in this region.

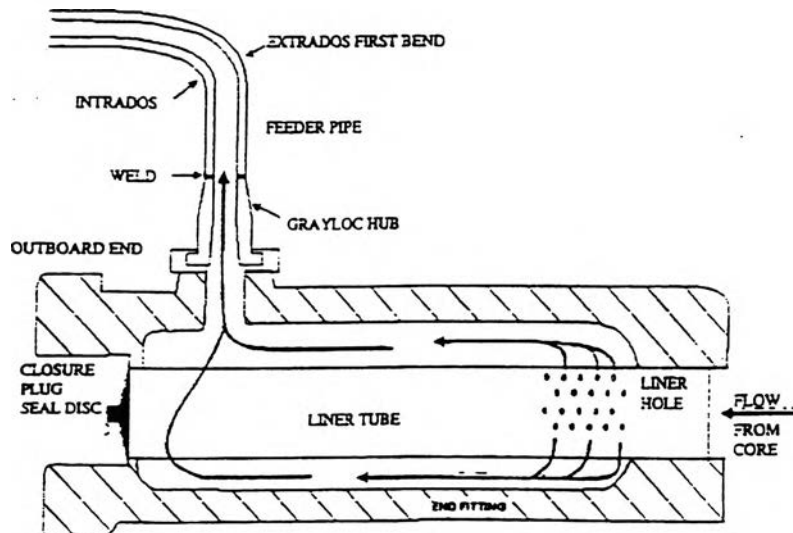


Figure 14: Flow Path Through the Endfitting, Grayloc Hub and First Bend of an Outlet Feeder [Cheluguet, 1997]

Figure 2.19 The entrance of outlet feeder pipe.

In 1963, Olson and Sparrow proposed the expression for pressure drop in ducts affected by entrance effects. It is a pressure drop at fully developed flow with the correction factor.

$$\frac{P_s - P}{\rho U^2 / 2} = \frac{fL}{D_h} + K \quad (2.26)$$

$$K = k_L - 1 \quad (2.27)$$

where P_s = pressure at upstream (inlet)
 P = pressure at distance L
 ρ = fluid density
 U^2 = mean velocity
 f = friction in fully developed flow
 L = distance from the duct entrance
 K = correlation factor
 D_h = hydraulic diameter
 k_L = the entrance loss effect.

Pressure drop was correlated with wall shear stress according to Eq. 2.28. Therefore the shear stress is also affected by the entrance correction factor.

$$\frac{-\Delta P}{L} = \frac{4\tau_w}{D} \quad (2.28)$$

2.8 Electrochemistry

Corrosion of metal in aqueous systems involves electrochemistry. It involves two or more electrochemical reactions on the metal surface. Electrochemical reactions are usually discussed in terms of the change in valence that occurs between the reacting elements (oxidation and reduction).

There are two kinds of reactions :

- 1) Cathodic reactions are the reactions that result in reduction. The reduction is the addition of electrons to an atom or group of atoms, consequently, resulting in decrease in valence. The location where the cathodic reaction takes place is called the cathode.

- 2) Anodic reactions are the reactions that result in oxidation. The oxidation is the removal of electrons from an atom or group of atoms. This results in the increase in valence. This kind of reaction takes place at the anode.

2.8.1 Nernst Equation

Thermodynamics is the basis that is used to determine the potentials of the electrodes. Thermodynamics concerns the chemical equilibrium and the driving forces for chemical reactions. Free energy is the thermodynamic property that provides the driving force and controls the spontaneous direction of the chemical reactions. The tendency of any chemical reaction to go can be measured by the Gibbs free energy (ΔG). The more negative value of ΔG , the greater tendency for the reaction to occur. If ΔG is positive, the reaction does not occur spontaneously.

The passage of a charge through the electrode causes the Gibbs free energy to change. The relationship between the free energy and voltage at electrode is expressed in Eq. 2.29.

$$|\Delta G| = \text{charge passed} \times \text{potential difference} \quad (2.29)$$

or
$$|\Delta G| = nF \times |E| \quad (2.30)$$

When the potential (E) is positive, the reaction will occur spontaneously as well as when Gibbs free energy is negative. Thus, Eq. 2.30 can be expressed as

$$\Delta G = -(nF \times E) \quad (2.31)$$

and
$$\Delta G^\circ = -(nF \times E^\circ) \quad (2.32)$$

where ΔG° = Gibbs free energy at standard state

E° = standard potential difference.

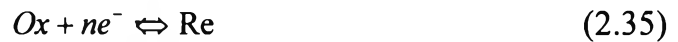
From the thermodynamic relationship

$$\Delta G = \Delta G^\circ + RT \ln K \quad (2.33)$$

Thus,

$$E = E^\circ - (RT/nF) \ln K \quad (2.34)$$

For reaction,



$$E_{O/R} = E_{O/R}^\circ - \frac{RT}{nF} \ln \frac{a_{Re}}{a_{Ox}} \quad (2.36)$$

$$E_{O/R} = E_{O/R}^\circ + \frac{RT}{nF} \ln \frac{a_{Ox}}{a_{Re}} \quad (2.37)$$

- where Ox = oxidized species
 Re = reduced species
 n = the number of electrons involved
 e⁻ = electron
 E_{O/R} = potential difference for reduction reaction
 E[°]_{O/R} = standard potential difference for reduction reaction
 R = gas constant
 T = absolute temperature
 a_{Ox} = activity of oxidized species
 a_{Re} = activity of reduced species
 K = equilibrium constant.

Eq. 2.37 is the well known “Nernst equation”. It indicates that the electrode potential change is a function of not only temperature and pressure, but also concentration. This electrode potential change determined by the Nernst equation is called the equilibrium potential.

2.8.2 Exchange Current Density

The amount of corroded metal or the amount of reacted substance is proportional to the amount of current. For corrosion reactions,

this current is called corrosion current. The relationship between mass and current, can be expressed as:

$$w = K \times it \quad (2.38)$$

where w = reacted mass (grams)

K = constant (grams/coulomb)

i = current (Amps)

t = time (seconds).

Eq. 41 obeys Faraday's law and can be rewritten as Eq. 2.39,

$$i_{\text{corr}} t = \frac{nFw}{MW} \quad (2.39)$$

where i_{corr} = corrosion current

nF = the number of coulombs(C) required to convert 1 mole of metal to corrosion product

n = the number of involved electrons

F = Faraday constant (96480 C/mol)

t = time (second)

w = corroded metal

MW = molecular weight of metal.

From Eq. 2.39,

$$rate(r) = \frac{w / MW}{tA} = \frac{1}{nFA} \quad (2.40)$$

For any reaction, rate of forward(r_f) equals rate of reverse(r_r) in the equilibrium state.

$$r_f = r_r = \frac{i_0}{AnF} \quad (2.41)$$

When rates of both forward and reverse are equal, the current at this condition is called the exchange current. If this current is divided by area (A), the new parameter is called the exchange current density(I_0).

$$I_0 = \frac{i_0}{A} \quad (2.42)$$

For any reaction, there is an energy of activation as shown in Figure 2.20.

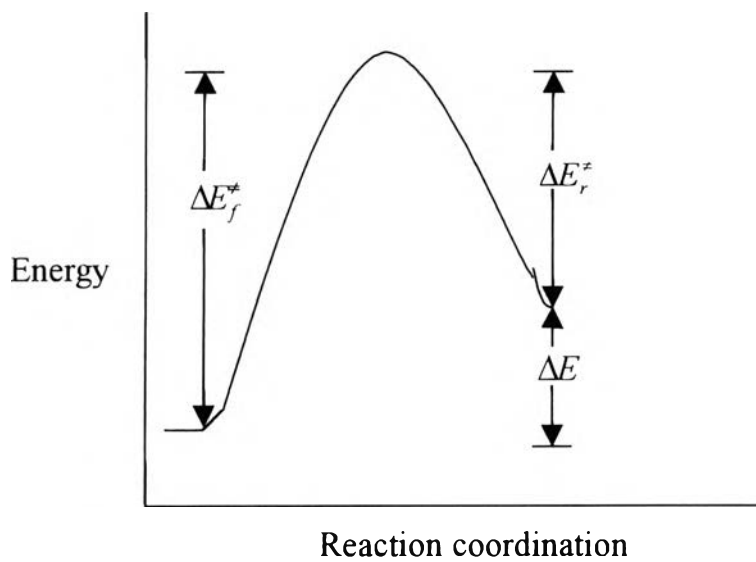


Figure 2.20 The overall energy of reaction.

The overall energy of reaction is given by

$$\Delta E_f^{\ddagger} - \Delta E_r^{\ddagger} = \Delta E \quad (2.43)$$

The Arrhenius relation,

$$k = A \exp(-\Delta E^{\ddagger} / RT) \quad (2.44)$$

Let $\Delta H^{\ddagger} \approx \Delta E^{\ddagger}$, multiply the right hand side of Eq. 2.43 by $\exp(-\Delta S/R)\exp(T\Delta S/RT)$. Then,

$$k = (A e^{-\Delta S^{\ddagger}/R})(e^{-\Delta H^{\ddagger}/RT} e^{T\Delta S^{\ddagger}/RT}) \quad (2.45)$$

$$= A' e^{-(\Delta H^{\ddagger} - T\Delta S^{\ddagger})/RT} \quad (2.46)$$

Eq. 2.45 and 2.46 are based on the thermodynamic relation,

$$\Delta G = \Delta H - T\Delta S \quad (2.47)$$

Hence,

$$k = k' \exp(-\Delta G^\ddagger / RT) \quad (2.48)$$

- where
- A = factor of frequency
 - ΔE_f^\ddagger = activation energy for forward reaction
 - ΔE_r^\ddagger = activation energy for reverse reaction
 - ΔE = energy change of reaction
 - k = rate constant
 - R = gas constant
 - T = absolute temperature
 - ΔH^\ddagger = enthalpy of activation
 - ΔS^\ddagger = activation entropy
 - ΔG^\ddagger = free energy of activation.

For the reduction reaction Eq. 2.38 yields

$$r_f = k_f C_O \quad (2.49)$$

$$= k' C_O \exp(-\Delta G_f^\ddagger / RT) \quad (2.50)$$

For the reverse reaction,

$$r_r = k_r C_R \quad (2.51)$$

$$= k' C_R \exp(-\Delta G_r^\ddagger / RT) \quad (2.52)$$

- where
- r_f = rate of forward reaction (reduction)
 - r_r = rate of reverse reaction (oxidation)
 - k_f = rate constant for forward reaction
 - k_r = rate constant for reverse reaction
 - C_O = concentration of oxidized species
 - C_R = concentration of reduced species
 - k' = constant
 - ΔG_f^\ddagger = free energy of activation for forward reaction
 - ΔG_r^\ddagger = free energy of activation for reverse reaction.

From Bockris (1972),

$$k = \frac{Fk''T}{h} \exp(-\Delta G_o^\ddagger / RT) \quad (2.53)$$

where k = jump frequency (frequency with which an ion successfully jumps energy barrier)

k'' = the number of times per second that the rate process occurs
(Boltzmann constant = 1.38×10^{-23} J K⁻¹)

h = Planck's constant = 6.62×10^{-34} J s .

Eq. 2.53 is based on reaction $Ox + e^- \rightleftharpoons Re$, where there is only one electron. If there are n involved electron(s), Eq. 2.53 can be rewritten to be

$$k = \frac{nFk''T}{h} \exp(-\Delta G^\ddagger / RT) \quad (2.54)$$

From Eq. 2.41, 2.42 and 2.54; yield

$$I_o = \frac{-nFk''T}{h} C_o \exp(-\Delta G_c^\ddagger / RT) = \frac{nFk''T}{h} C_R \exp(-\Delta G_a^\ddagger / RT) \quad (2.55)$$

where ΔG_c^\ddagger = free energy of activation for cathodic reaction

ΔG_a^\ddagger = free energy of activation for anodic reaction.

When there is interfacial potential difference, the electric field will occur across the interface and the work done by an ion climbing the potential-energy barrier has to involve the electrical work. Therefore, the free energy of activation depends not only on the chemical reaction but also the potential difference (E). This electrical work done is the potential difference multiplied by the charge (nF).

For reduction reactions, presumably for forward reaction, the free energy of activation increases with the potential difference effect. Thus, free energy is:

$$\Delta G_c^\ddagger = \Delta G_{0,c}^\ddagger + \alpha_c nFE \quad (2.56)$$

For oxidation, this potential difference results in a lowered free energy of activation.

$$\Delta G_a^{\ddagger} = \Delta G_{0,a}^{\ddagger} - \alpha_a nFE \quad (2.57)$$

where $\Delta G_{0,c}^{\ddagger}$ = free energy of activation for cathodic reaction caused by chemical reaction

$\Delta G_{0,a}^{\ddagger}$ = free energy of activation for anodic reaction caused by chemical reaction

α_c = cathodic transfer coefficient

α_a = anodic transfer coefficient.

$$\alpha_a + \alpha_c = 1 \quad (2.58)$$

Let $\beta = \alpha_c$ and $(1 - \beta) = \alpha_a$

Therefore, Eq. 2.55 is rewritten as;

$$I_0 = -nF \frac{k''T}{h} C_o \exp(-\Delta G_{0,c}^{\ddagger} / RT) \exp(-\beta nFE_e / RT) \quad (2.59)$$

$$I_0 = nF \frac{k'T}{h} C_R \exp(-\Delta G_{0,a}^{\ddagger} / RT) \exp((1 - \beta)nFE_e / RT) \quad (2.60)$$

where E_e = equilibrium potential.

2.8.3 Butler Volmer Equation

There are two types of reaction in the system, so there are two types of current in the system: cathodic current and anodic current. The absolute current is the sum of both current.

$$i = |i_a| + |i_c| \quad (2.61)$$

$$= i_a - i_c$$

$$(2.62)$$

i_c , cathodic current, results from the reduction reaction at the cathode(-). This current is negative, so it is subtracted from i_a , the anodic current as Eq. 2.62.

If areas for both reactions are the same,

$$I = I_a - I_c \quad (2.63)$$

$$I_a = kC_R \exp((1 - \beta)nFE_e / RT) \quad (2.64)$$

Multiply rhs of Eq. 2.63 by $\exp((1-\beta)nFE_e/RT)\exp(-(1-\beta)nFE_e/RT)$

Then,

$$I_a = I_0 \exp((1 - \beta)nF(E - E_e) / RT) \quad (2.65)$$

$$I_a = I_0 \exp((1 - \beta)nF\eta / RT) \quad (2.66)$$

where:

$$\eta = \text{overpotential}$$

For cathodic,

$$I_c = -I_0 \exp(-\beta nF\eta / RT) \quad (2.67)$$

From Eq. 2.63,

$$I = I_0 [\exp((1 - \beta)nF\eta / RT) - \exp(-\beta nF\eta / RT)] \quad (2.68)$$

Eq. 2.68 is known as the “Butler-Volmer equation”. When the overpotential is sufficiently large, one reaction occurs at a negligible rate, and the overpotential is then in the Tafel expression form.

Tafel reaction;

$$\eta = a + b \log i \quad (2.69)$$

As the overpotential is much negative, I_c increases while I_a decreases. Thus, $|I_c| \gg |I_a|$. Then Eq. 2.68 is reduced to;

$$I = -I_0 \exp(-\beta nF\eta / RT) \quad (2.70)$$

$$\eta_c = -\frac{RT}{\beta nF} \ln \frac{I}{I_0} = -\frac{2.303RT}{\beta nF} \log \frac{I}{I_0} \quad (2.71)$$

This equation is known as the cathodic Tafel equation. At positive overpotential, $|I_a| \gg |I_c|$, the anodic Tafel equation is obtained,

$$\eta_a = \frac{RT}{(1 - \beta)nF} \ln \frac{I}{I_0} = \frac{2.303RT}{(1 - \beta)nF} \log \frac{I}{I_0} \quad (2.72)$$

2.8.4 Mixed Potential

There are two or more different reactions in the system, and these reactions are divided into cathodic and anodic as mentioned in the beginning of section 2.8.

These reactions affect the overall current or corrosion current and overall potential or corrosion potential.

Total anodic current equals total cathodic current

$$i_{corr} = \sum i_{anodic} = \sum i_{cathodic} \quad (2.73)$$

where i_{corr} = corrosion current

i_{anodic} = anodic current

$i_{cathodic}$ = cathodic current.

If there are two reactions in the system,

$$i_M = -i_{so} = i_{corr} \quad (2.74)$$

where i_M = metal dissolution current

i_{so} = electronation current.

$$i_M = A_M I_M \quad (2.75)$$

$$= A_M I_{0,M} \left[\exp((1 - \beta_M) nF \eta / RT) - \exp(-\beta_M nF \eta / RT) \right] \quad (2.76)$$

$$= A_M I_{0,M} \left[\exp\left(\frac{E_{corr} - E_{e,M}}{\bar{\alpha}_M}\right) - \exp\left(-\frac{E_{corr} - E_{e,M}}{\bar{\alpha}_M}\right) \right] \quad (2.77)$$

$$-i_{so} = -A_{so} I_{0,so} \left[\exp((1 - \beta_{so}) nF \eta / RT) - \exp(-\beta_{so} nF \eta / RT) \right] \quad (2.78)$$

$$= A_{so} I_{0,so} \left[\exp\left(-\frac{E_{corr} - E_{e,so}}{\bar{\alpha}_{so}}\right) - \exp\left(\frac{E_{corr} - E_{e,so}}{\bar{\alpha}_{so}}\right) \right] \quad (2.79)$$

Assume $\bar{\alpha}_M = \bar{\alpha}_{so}$ and $\bar{\alpha}_{so} = \bar{\alpha}_{so}$

If $A_M = A_{so}$, and with Eq. 2.74,

$$I_{corr} = I_{0,M} \left[\exp\left(\frac{E_{corr} - E_{e,M}}{\bar{\alpha}_M}\right) - \exp\left(-\frac{E_{corr} - E_{e,M}}{\bar{\alpha}_M}\right) \right] \quad (2.80)$$

$$= I_{0,so} \left[\exp\left(-\frac{E_{corr} - E_{e,so}}{\bar{\alpha}_{so}}\right) - \exp\left(\frac{E_{corr} - E_{e,so}}{\bar{\alpha}_{so}}\right) \right] \quad (2.81)$$

Assume $\beta = 1 - \beta = 0.5$

$$E_{corr} = \frac{RT}{nF} \ln \frac{I_{0,so} e^{nFE_{e,so}/2RT} + I_{0,M} e^{nFE_{e,M}/2RT}}{I_{0,so} e^{-nFE_{e,so}/2RT} + I_{0,M} e^{-nFE_{e,M}/2RT}} \quad (2.82)$$

Figure 2.21, Evans diagram, illustrates the relationship of current and potential for corrosion process.

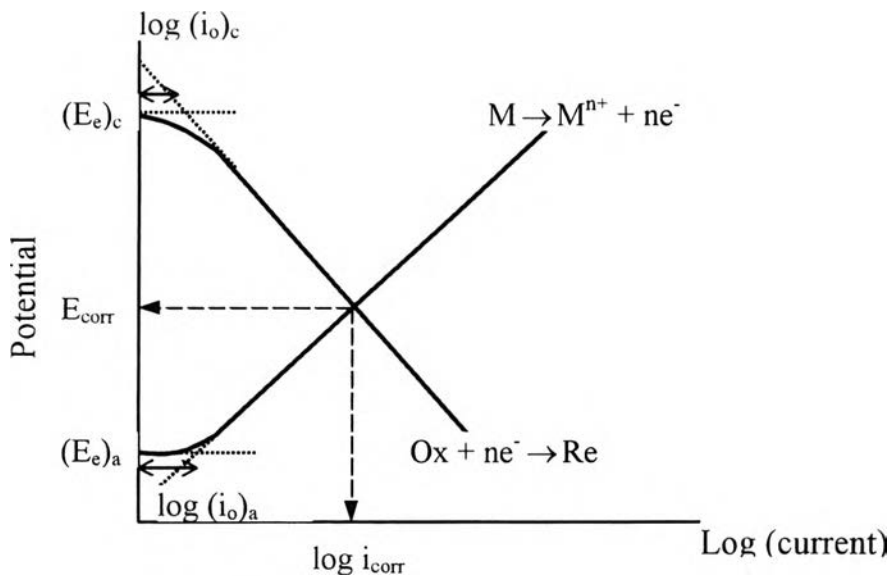


Figure 2.21 Evans diagram for corrosion process $M + Ox \rightarrow M^{n+} + Re$.

2.8.5 The Effect of Mixed Potential

The mixed potential is caused by the cathodic reaction and the anodic reaction. In corrosion systems of outlet feeders, there are two interesting locations that are considered for mixed potentials. The first is the mixed potential at metal/oxide interface which can be called corrosion potential, and the second one is mixed potential at the oxide/solution interface.

The mixed potential affects the iron ion solubility. The local solubility can be adjusted by the mixed potential equation (Eq. 2.82) and the Nernst equation (Eq. 2.37). Additionally, the dissolution rate and precipitation

rate or oxide growth rate are affected by the local mixed potential (Mancey, 1997).

$$k_{d,adj} = k_d \exp\left(\frac{(1-\beta)nFE}{RT}\right) \quad (2.83)$$

$$k_{p,adj} = k_p \exp\left(\frac{-\beta nFE}{RT}\right) \quad (2.84)$$

where $k_{d,adj}$ = adjusted dissolution rate constant by electrochemical effect
 k_d = dissolution rate constant
 $k_{p,adj}$ = adjusted precipitation rate constant by electrochemical effect
 k_p = precipitation rate constant.

Solubility(C_{sol}) at the metal/oxide interface is adjusted by using the Nernst equation and the wall concentration affected by the local mixed potential can be determined by Eq. 2.86 with the assumption that the precipitation rate equals the rate of oxide growth.

$$\text{Fe}^{2+} \text{ precipitation} = \text{Fe}^{2+} \text{ in the oxide growth rate} \quad (2.85)$$

$$k_p F^* (C_w - C_{sol}) = 0.476 \frac{dm}{dt} (1 - \phi) \quad (2.86)$$

Thus,

$$C_w = C_{sol} + 0.476 \frac{dm}{dt} (1 - \phi) \frac{1}{k_p F^*} \quad (2.87)$$

where C_w = iron dissolved concentration at wall
 C_{sol} = solubility of iron dissolved
 ϕ = porosity
 k_p = precipitation rate constant
 F^* = surface area factor ($=\sqrt{3}$ for octahedra (Lister, Arbeau, and Johari, 1994))
 $\frac{dm}{dt}$ = rate of mass loss.

About the effect of mixed potential on dissolution, Allen *et al.* (1981) found that the effect of mixed potential on dissolution of magnetite is different

at different pH. They thought this difference resulted from two processes: 1) the protonation of the electrode surface and 2) an enhanced rate of reduction of the oxide surface.